Published in final edited form as:

J Phys Chem C Nanomater Interfaces. 2011 February 24; 115(7): 2999–3004. doi:10.1021/jp111244v.

Resistive Pulse Analysis of Microgel Deformation During Nanopore Translocation

Deric A. Holden[1], **Grant Hendrickson**[2], **L. Andrew Lyon**[2,*], and **Henry S. White**[1,*]

[1]Department of Chemistry, University of Utah, 315 S 1400 E, Salt Lake City, UT 84112

[2]Georgia Institute of Technology, School of Chemistry and Biochemistry and Petit Institute for Bioengineering & Bioscience, 901 Atlantic Drive, NW, Atlanta, GA 30332-0400

Abstract

Deformation of 570-nm radius poly(N-isopropylacrylamide-co-acrylic acid) microgels passing through individual 375- to 915-nm radius nanopores in glass has been investigated by the resistive-pulse method. Particle translocation through nanopores of dimensions smaller than the microgel yields electrical signatures reflecting the dynamics of microgel deformation. Translocation rates, and event duration and peak shape, are functions of the conductivities of microgel and electrolyte. Our results demonstrate that nanopore resistive-pulse methods provide new fundamental insights into microgel permeation through porous membranes.

Keywords

Microgel; nanopore; resistive pulse

We report investigations of the deformation of microgels as they are driven at low applied pressures through a nanopore in a thin glass membrane. Translocation of soft, deformable particles through small orifices is of interest due to the growing realization that nanoparticle mechanical properties play an important role in biological processes such as cellular uptake, organ localization, extravasation into tumors, and excretion.[1,2] Hendrickson and Lyon recently reported pressure-driven translocation of microgels through a polymeric, track-etched membrane containing a high density of cylindrical pores.[3] In those experiments, microgels were driven through nanopores with diameters tenfold smaller than the unperturbed particle diameter, under hydrostatic pressures relevant to renal filtration. Translocation of a large, soft, hydrated particle through a small pore requires significant deformation, and perhaps dehydration of the particle, and is thus anticipated to be a function of the particle's materials properties, the size of the particle and pore, and the surface forces between particle and pore (e.g., electrostatic forces). The mechanism by which a soft polymeric particle enters into a nanopore, deforms to the pore geometry, and passes through the pore interior is virtually unexplored. While the above-mentioned investigations using track-etched membranes demonstrated microgel translocation through small pores, they do

* lyon@gatech.edu; white@chem.utah.edu.

Supporting Information Available: Examples of blocked pore signals and the definition of the time interval dt used in the Poisson analysis. This material is available free of charge via the Internet at http://pubs.acs.org.

not provide direct insight into the mechanism of microgel deformation during translocation. Herein, we demonstrate that resistive-pulse methods can be used to investigate microgel translocation, providing a means to directly measure the dynamics of single particle deformation from electrical current-time (*i*-*t*) traces.

Resistive-pulse techniques have been used for decades to count and measure the size of particles, in addition to measuring particle-pore interactions.[4-8] These methods are based on measuring a decrease in the ionic current that occurs when the particle, driven by pressure or electrophoretic forces, passes through an opening or channel connecting two electrolyte solutions. For solid particles, translocation occurs only when the particle size is smaller than the pore, whereas a method based on particle "capture and release" has been proposed for detection of solid particles that are larger than the opening.[9] In addition, translocation of small molecules and biomolecules through synthetic and biological nanopores has been extensively investigated using the resistive-pulse technique.[10-18] The conformational flexibility of macromolecules, especially biopolymers, facilitates entry into the pore. For example, Fologea et al. demonstrated that ssDNA translocates through a 4-nm radius solid-state nanopore both in folded or unfolded states, producing conformation-dependent signatures in the ionic current. Similarly, the electric-field driven translocation of ssDNA through a protein with a very small pore opening (e.g., α-hemolysin) requires threading of the end of the DNA molecule into the protein, followed by unfolding of the DNA secondary structure as the molecule passes linearly, base-by-base, through the protein channel.

RESULTS AND DISCUSSION

The deformation of 570-nm radius poly(N-isopropylacrylamide-co-acrylic acid) (pNIPAm-AAc) microgels during translocation was investigated using glass nanopore membranes (GNM). A schematic diagram of the experimental setup used to investigate microgel deformation during translocation is shown in Figure 1. The GNM is a ~50 μm-thick soda-lime glass membrane containing a single conically-shaped pore; the membrane is located at the end of a glass capillary, separating internal and external electrolyte solutions. The radii of the small orifice of GNMs used in this investigation were determined by measuring the nanopore conductance in a 1 M KCl solution.[19] A pressure of −50 mmHg was applied across the nanopore (internal vs. external) using a gas tight syringe attached to the capillary, creating a pressure-driven flow of the external electrolyte solution and particles through the nanopore. A constant potential of +0.1 V was applied between two Ag/AgCl electrodes, one positioned in the internal solution and the other located in the external solution. The purpose of the applied voltage is to generate an ionic current through the pore for sensing particle translocation. The applied voltage also generates an electrophoretic force on the negatively charged pNIPAm-AAc microgels, but, as observed experimentally, this force is insufficient to drive the particles through the pore in the absence of an applied pressure, as measured over a range of the pressures and applied voltages (data not presented). Thus the pressure-driven convective flow determines the particle flux through the nanopore. The results reported herein are independent of the sign of the applied voltage.

PNIPAm-AAc microgels were synthesized as previously described,[3] and were dispersed at 0.001 wt% in buffered KCl solutions (10 to 130 mM). The average microgel hydrodynamic

radius in a 10 mM PBS buffer (100 mM ionic strength, pH 7.4) solution is 570 nm, as determined by dynamic light scattering (DLS).[3] The ζ-potential in low ionic strength buffers of pH 7.4 and pH 3.0 was determined to be −20.5 mV and −4.1 mV, respectively, by electrophoretic light scattering. Note that the ζ-potential should not be considered to originate at the microgel surface charge since the "surface" of a microgel is an ill-defined plane. It is almost certainly the case that partially buried charges within the microgel surface can contribute to the observed mobility. However, ζ-potential values do provide a measure of the relative degree of charging between different microgels or different solution conditions. The microgel acrylic acid concentration was estimated to be ~0.01 M based on AAc synthesis concentration, hydrodynamic radius, and the approximate molecular weight. At pH 7, monomer AAc groups are largely deprotonated (>99.8%, pKa of ~4.25), and are Coulombically balanced by the mobile K^+ from the buffer electrolyte. Thus, the conductivity of the microgel is significant, although the net charge is low.

A microgel passing through the orifice of the pore displaces the electrolyte solution, resulting in a deviation in the pore conductance. The corresponding transient pulse in the *i-t* trace indicates translocation of an individual microgel through this volume. Finite-element simulations demonstrate that the majority of the nanopore resistance (i.e., the sensing zone) is localized to the volume of solution within a few radii of the pore orifice, a consequence of the radially divergent field on both sides of the orifice.[9]

Translocation experiments were performed using GNMs with orifice radii ranging between 73- and 915-nm. Figure 2 shows *i-t* traces recorded in a buffered 10 mM KCl solution for the translocation of the 570-nm radius microgel particles through a 433-nm radius GNM. The shape of the resistive pulse reflects the entry and passage of the particle through the nanopore. Particles driven by convective flow from the bulk external solution encounter the pore orifice on the GNM surface and displace the electrolytic solution, causing the current to *increase* from the baseline value. The observation that the current increases during translocation indicates that the microgel has a higher conductivity that the electrolyte solution, as discussed in more detail below. As the particle deforms under pressure and enters the pore, it begins to fill the interior volume of the pore, resulting in a microgel structure that is pinched down at the orifice (see Figure 1). Continued passage of the particle into the expanding nanopore volume allows the particle to relax to its original unconstrained spherical shape. The translocation time ($\Delta\tau$) is defined as the width of the resistive peak at half height, and the resistive-pulse magnitude (Δi) is measured from the baseline i_o, the latter corresponding to the unblocked pore.

In order to verify the resistive-pulses correspond to successful translocations and not to failed entry attempts, we performed experiments in which the pressure, *P*, across the nanopore was reversed following a period of time in which resistive-pulses were observed. If a resistive-pulse at -*P* corresponds to a successful translocation, then reversing the direction of electrolyte flow drives the same particle back through the nanopore in the reverse direction at +*P*, producing a corresponding resistive pulse at a later time. Figure 3 shows results of this experiment for a 466-nm radius nanopore. Particles were initially placed outside the pore. A positive pressure of +50 mmHg was applied to the interior of the capillary inducing an outward flow of solution and subsequent steady background signal.

The pressure was then reversed to −50 mmHg, driving ~400 particles through the pore and into in the inner solution. After ~9 s, the pressure was reversed to +50 mmHg and the captured particles were then pushed back out of the pore, once more passing through the pore orifice and detected a second time. At about 25 s, all the particles had passed back through the pore and events were no longer observed. The *i*-*t* traces for all pores larger than ~375-nm showed forward and reverse translocation for microgel particles with approximately the same number of events recorded before and after pressure reversal. Experiments using GNMs of radii less than 375 nm resulted in pulses in the *i*-*t* traces at negative pressure, but the corresponding translocation pulses at positive pressure were not observed. These events correspond to attempted entry of microgels into the nanopore, transiently blocking the pore orifice but resulting in unsuccessful translocation. Additionally, using pores smaller than 375-nm, microgels were occasionally "captured" for long durations, require reversal of the pressure to dislodge them from the pore mouth (see Supporting Information) As shown in Figure 3, some *i*-*t* traces contain a very small number of events corresponding to a decrease in current from the baseline. We speculate that these events correspond to contaminate particles due to their occasional appearance in background traces, as well as in solutions containing the microgels (Figure 2).

Previously, Hendrickson and Lyon reported a particle-to-pore ratio as large as 10 for observing translocation of the 570-nm radius microgels through track-etched polycarbonate membranes, corresponding to translocation through pores significantly smaller than those employed in the current experiments.[3] We speculate that the negative surface charge at the glass nanopore opening provides a sufficient barrier to passage of the anionic microgels, as opposed to the approximately neutral surface charge of the track-etched polycarbonate membrane pores. Studies of the effects of particle/pore interactions on particle translocation using the resistive-pulse technique are currently underway.

Additionally, resistive-pulses associated with particle translocation through GNMs with radii greater than 700-nm were not distinguishable from the background current i_o due to the inability to detect the small change in conductivity between the particle and the surrounding solution in a large sensing volume. Additionally, translocation times decrease with increasing pore size due to decreased particle-pore interactions and events may be too fast to be monitored using the current instrumental setup. Reproducible translocation events were observed using GNMs with radii between 375- and 618-nm; background *i*-*t* traces showed no peaks above noise when particles were not present in solution.

A plot of the particle translocation rate as a function of pore size is shown in Figure 4 for pores sizes between 73- and 618-nm. As previously discussed, translocation events are not observed for pore sizes below 375-nm; however a sharp increase in event rate occurs (0 to ~50 s^{-1}) above 375-nm. Above this threshold radius, event rates increase proportionally to the third power of the nanopore radius (a^3), in agreement with the dependence of the volumetric flow rate on the radius. However, as shown in Figure 4, the observed event rate is significantly lower than expected (only 4.2% of theory), although still following the a^3 dependence. This observed low event rate is most likely due to the electrostatic repulsion between the negatively charged GNM and the negatively charged microgel, inhibiting the ability for the microgel to translocate the GNM. As noted above, translocation through pores

with radii greater than 700-nm were also observed, but were difficult to discern above the open pore noise. Thus, event rates for these pores cannot be accurately determined.

In a 10 mM KCl buffered solution, an increase in the ionic current was observed during 570-nm radius microgel translocation. This increase in current can be understood by considering the ionic conductivity of the microgel relative to the conductivity of the solution volume displaced during translocation. The microgel itself is a porous structure with an estimated AAc concentration of ~0.01 M. As previously mentioned, at pH 7 nearly all of the acrylic acid groups are dissociated and are charged balanced by mobile K^+. As the particle passes though the pore, the 10 mM electrolyte solution is displaced by the particle, producing an increase in the current due to the higher conductivity of the particle. A quantitative description of the current increase will require a detailed understanding of not only the nanopore surface charge density, but also the activities and mobilities of the fixed (polymer bound) and mobile ions contained within the microgel.

We further explored the shape of the resistive-pulse on the relative ionic concentrations of the microgel and bulk solution by measuring microgel translocation events using a 433-nm pore in electrolyte containing between 10 mM to 130 mM KCl, at pH 7. Resulting translocation times and current deviations are shown in Figure 5. Translocation times decreased as ionic concentration increased. The increased ionic concentration causes deswelling of the particles from a radius of 610-nm at 10 mM KCl to a radius of 518-nm in 130 mM KCl, as determined by DLS. As the particle radius decreases, it requires less interaction and deformation to translocate a pore, resulting in shorter translocation times. In addition, as the bulk solution ionic strength increases, the microgel charges are screened more effectively, thereby lowering the deformation barrier to passage. As noted above, translocation is driven primarily by pressure-induced fluid convection and not by electrophoretic forces; thus, increased electrostatic shielding has little effect on the translocation. A lower limit of $\Delta\tau$ ~50 μs for KCl concentrations greater than 60 mM KCl (see Figure 5(a)) results from the 10 kHz low-pass filter of the electronic instrumentation.

Pulse-heights as a function of the electrolyte concentration are shown in Figure 5(b). The magnitude and sign of the current-pulse is related to the conductance of the particle relative to the electrolyte that the particle displaces during translocation. Figure 5(b) shows that at low electrolyte concentrations, particle translocation results in an increase in the current corresponding to a higher particle conductance relative to the surrounding solution. Conversely, at high electrolyte concentration, a decrease in current is observed during translocation corresponding a relatively lower particle conductance. By interpolating pulse heights to $\mu i = 0$, the equivalent conductivity of the particle can be estimated. In this case, the microgels have an ionic conductivity equivalent to a 48 mM KCl solution.

In most *i*-*t* traces, the resistive-pulse magnitudes, μi, are nearly uniform (< ±0.2%). However, in some instances (see Figure 3) variable peak-heights were observed. In order to determine if these anomalous events are coincident events or correspond to particle aggregates, a Poisson statistical analysis of the probability of overlapping particle translocation events was performed, following the method described by Davis and Giddings[20,21] for determining the probability of coincident overlap of chromatographic

peaks. Poisson statistics yield the probability of uncorrelated particle translocation events, λ, that occur during a total observation time, T. The expected number of translocation events, m, in an observation time is given by the equation:

$$m=\lambda T. \quad (1)$$

Because the translocation events are of finite duration and occur stochastically, there is a finite probability that two or more events will overlap and be counted as a single event. Thus, the observed number of events may be smaller than the actual number of particles that translocate through the pore.

The probability of single, double, or n-component events is determined as follows. First, the observed events in an observation time T are counted. The time separating the mid-point of two consecutive events is defined as dt (See Supporting Information). The probability that dt is greater than the time necessary to resolve these events with baseline resolution, to (~300 μs), is given by

$$p\left(\mathrm{d}t>t_{\mathrm{o}}\right)=exp\left(-\lambda t_{\mathrm{o}}\right). \quad (2)$$

Multiplication of p(dt > t_{o}) by m, followed by substitution of $\lambda = m/T$ (from eq 1), yields the number (N) of time intervals between observed events with dt > t_{o} as a function of t_{o}:

$$N=mexp\left(-mt_{\mathrm{o}}/T\right). \quad (3)$$

Rearranging eq 3 yields:

$$ln\left(N\right)=ln\left(m\right)-m\left(t_{\mathrm{o}}/T\right) \quad (4)$$

The expected number of observed events, m, is determined by plotting ln(N) as a function of t_{o}/T (see Figure 6). Both the slope (-m) and the intercept (ln(m)) yield m. For the i-t data shown in Figure 2(b), m was determined to be 427 and 431, from the slope and intercept, respectively, in excellent agreement with the actual number of observations, 443.

The probability that an individual event represents 1, 2, 3, …, n particle translocation events is given by:

$$N_{\mathrm{n}}=exp\left(-2mt_{\mathrm{o}}/T\right)\left[1-exp\left(-mt_{\mathrm{o}}/T\right)\right]^{(n-1)} \quad (5)$$

Analysis of the data set presented in Figure 2(b) yields a 99.6% probability of any resistive-pulse being a single event. Similarly, the probability of coincident events is negligibly small (the probabilities for double and triple events are 2.1×10^{-3} and 4.4×10^{-6}, respectively), in agreement with the general observation of peaks of uniform magnitude. Thus, an event with

an anomalously large peak height likely corresponds to a particle aggregate. Specifically, this was observed when using new samples in which the microgel had not been sufficiently re-dispersed, or older samples in which particles had aggregated.

Finally, Figure 7 shows a cluster plot of $\mu i/i_o$ vs. $\Delta\tau$ (bottom left) for the translocation of the 570-nm microgels using GNMs of 375, 509, and 618 nm radius. Histograms showing the distribution of $\Delta\tau$ and $\mu i/i_o$ for the same data sets are shown on the top left and bottom right, respectively. The histograms and cluster plot show reasonably sharp distributions of $\mu i/i_o$ and $\Delta\tau$, reflecting the uniformity of microgel translocation events. The ~15% distribution in $\mu i/i_o$ observed in Figure 7 primarily reflects the true size distribution of the microgel particles determined by DLS (about 10%)[3], in addition to possible spread caused by the mechanical deformation of the microgel as it passes through the pore. An increase in both the average $\Delta\tau$ and $\mu i/i_o$ was observed as the pore size decreases. For pore sizes 618-, 509-, and 375-nm, $\Delta\tau$ = 89 ± 17, 98 ± 11, and 117 ± 13 and $\mu i/i_o$ = 0.0045 ± 0.0008, 0.007 ± 0.001, and 0.011 ± 0.001, respectively. The decrease in pore size requires an increase in microgel deformation and interaction with the pore, while also increasing the microgel's occupation of the pore's sensing zone, resulting in both longer $\Delta\tau$ and larger $\mu i/i_o$. The results demonstrated that the resistive-pulse method is able to distinguish different particle-pore interactions.

CONCLUSIONS

We have demonstrated the use of the resistive-pulse method to investigate the kinetics and deformation dynamics of microgel translocation through nanopores. The capability enables a better understanding of the mechanisms and figures of merit for microgel passage through small orifices. Importantly, this approach provides the opportunity to follow individual events in real time, thereby resulting in data that can be directly correlated with the polymer physics and chemistry of individual microgels. Additionally, the relevance of such deformation events in the development of new drug delivery vehicles is critical; this experimental framework will provide tremendous insight into the design criteria for particles that are able to translocate across biological pores and through tight junctions.

EXPERIMENTAL METHODS

Solutions

All solutions were prepared in water obtained from a Barnstead E-pure purification system (>18 M μ cm). All chemicals, including KCl, K_2HPO_4, and KH_2PO_4 (Mallinckrodt Chemicals), were used without further purification.

570-nm-radius microgels

Poly(N-isopropylacrylamide-co-acrylic acid) microgels were originally prepared and sized by a process described elsewhere.[3] Samples were initially freeze-dried and then re-dispersed at 0.001 wt% in buffered KCl solutions.

Translocation experiments

All experiments were performed by using a Glass Nanopore Membrane, prepared by a process previously explained.[19] The internal and external solutions of the capillary contained buffered KCl solution. A constant potential of +0.1 V was applied between two Ag/AgCl electrodes, one positioned in the internal solution and the other located in the external solution. The current was measured by a Dagan Cornerstone Series Chem-Clamp voltameter/amperometer, using a high-sensitivity preamplifier (0.05 to 10 nA/V) and filtered using a 10 kHz 3-pole low-pass Bessel Filter. The instrument was interfaced to a PC through a BNC 2120 board (National Instruments) and a PCI 6251 DAQ card (National Instruments). Data was recorded at 150 kHz using in-house virtual instrumentation written in LavVIEW 8.6 (National Instruments). A pressure of −50 mmHg was applied across the nanopore (internal vs. external) using a gas tight syringe attached to the capillary.

Supplementary Material

Refer to Web version on PubMed Central for supplementary material.

Acknowledgment

This research was supported by the National Science Foundation (CHE-0616505) and by the National Institutes of Health (1 R01 GM088291-01). We thank Mr. Wen-Jie Lan (U. of Utah) for helpful discussions.

References

1. Mitragotri S, Lahann J. Physical approaches to biomaterial design. Nat. Mater. 2009; 8(1):15–23. [PubMed: 19096389]
2. Nel AE, Madler L, Velegol D, Xia T, Hoek EMV, Somasundaran P, Klaessig F, Castranova V, Thompson M. Understanding biophysicochemical interactions at the nano-bio interface. Nat. Mater. 2009; 8(7):543–557. [PubMed: 19525947]
3. Hendrickson GR, Lyon LA. Microgel Translocation through Pores under Confinement. Angew. Chem. Int. Ed. 2010; 49:2193–2197.
4. Ito T, Sun L, Bevan M, Crooks RM. Comparison of Nanoparticle Size and Electrophoretic Mobility Measurements Using a Carbon-Nanotube-Based Coulter Counter, Dynamic Light Scattering, Transmission Electron Microscopy, and Phase Analysis Light Scattering. Langmuir. 2004; 20:6940–6945. [PubMed: 15274607]
5. Petrossian L, Wilk SJ, Joshi P, Goodnick SM, Thornton TJ. Demonstration of Coulter counting through a cylindrical solid state nanopore. J. Phys. Conf. Ser. 2008; 109:012028.
6. Piruska A, Gong M, Sweedler JV, Bohn PW. Nanofluidics in chemical analysis. Chem. Soc. Rev. 2010; 39:1060–1072. [PubMed: 20179825]
7. Giehart BC, Howitt DG, Chen SJ, Zhu Z, Kotecki DE, Smith RL, Collins SD. Nanopore with transverse nanoelectrodes for electrical characterization and sequencing of DNA. Sens. Actuators B. 2008; 132:593–600.
8. Henriquez RR, Ito R, Sun L, Crooks RM. The Resurgence of Coulter Counting for Analyzing Nanoscale Objects. Analyst. 2004; 129:478–482. [PubMed: 15222315]
9. Lee S, Zhang Y, Harrell CC, Martin CR, White HS. Electrophoretic Capture and Detection of Nanoparticles at the Opening of a Membrane Pore Using Scanning Electrochemical Microscopy. Anal. Chem. 2004; 76:6108–6115. [PubMed: 15481960]
10. Fologea D, Gershow M, Ledden B, McNabb DS, Golovchenko JA, Li J. Detecting Single Stranded DNA with a Solid State Nanopore. Nano Lett. 2005; 5:1905. [PubMed: 16218707]
11. Han A, Schurmann G, Mondin G, Bitterli RA, Hagelbach NG, de Rooij NF, Staufer U. Sensing protein molecules using nanofabricated pores. Appl. Phys. Lett. 2006; 88:093901.

12. Bayley H, Martin CR. Resistive-Pulse Sensing From Microbes to Molecues. Chem. Rev. 2000; 100:2575–2594. [PubMed: 11749296]

13. Choi Y, Baker LA, Hillebrenner H, Martin CR. Biosensing with conically shaped nanopores and nanotubes. Phys. Chem. Chem. Phys. 2006; 8:4976–4988. [PubMed: 17091150]

14. Harrell CC, Choi Y, Horne LP, Baker LA, Siwy ZS, Martin CR. Resistive-Pulse DNA Detection with a Conical nanopore Sensor. Langmuir. 2006; 22:10837–10843. [PubMed: 17129068]

15. Sexton LT, Horne LP, Sherrill SA, Bishop GW, Baker LA, Martin CR. Resistive-Pulse Studies of Proteins and Protein/Antibody Complexes Using a Conical Nanotube Sensor. J. Am. Chem. Soc. 2007; 129:13144–13152. [PubMed: 17918938]

16. Sexton LT, Mukaibo H, Katira P, Hess H, Sherrill SA, Horne LP, Martin CR. An Adsorption-Based Model for Pulse Duration in Resistive-Pulse Protein Sensing. J. Am. Chem. Soc. 2010; 132:6755–6763. [PubMed: 20411939]

17. Deamer DW, Branton D. Characterization of Nucleic Acids by Nanopore Analysis. Acc. Chem. Res. 2002; 35:817–825. [PubMed: 12379134]

18. Baley H. Sequencing Single Molecules of DNA. Curr. Opin. Chem. Biol. 2006; 10:628–637. [PubMed: 17113816]

19. Zhang B, Galusha J, Shiozawa PG, Wang G, Bergren AJ, Jones RM, White RJ, Ervin EN, Cauley CC, White HS. Bench-Top Method for Fabricating Glass-Sealed Nanodisk Electrodes, Glass Nanopore Electrodes, and Glass Nanopore Membranes of Controlled Size. Anal. Chem. 2007; 79:4778–4787. [PubMed: 17550232]

20 (a). Davis JM, Giddings JC. Statistical theory of component overlap in multicomponent chromatograms. Anal. Chem. 1983; 55:418–424.

21. Giddings, JC. Unified Separation Science. Wiley; New York: 1991.

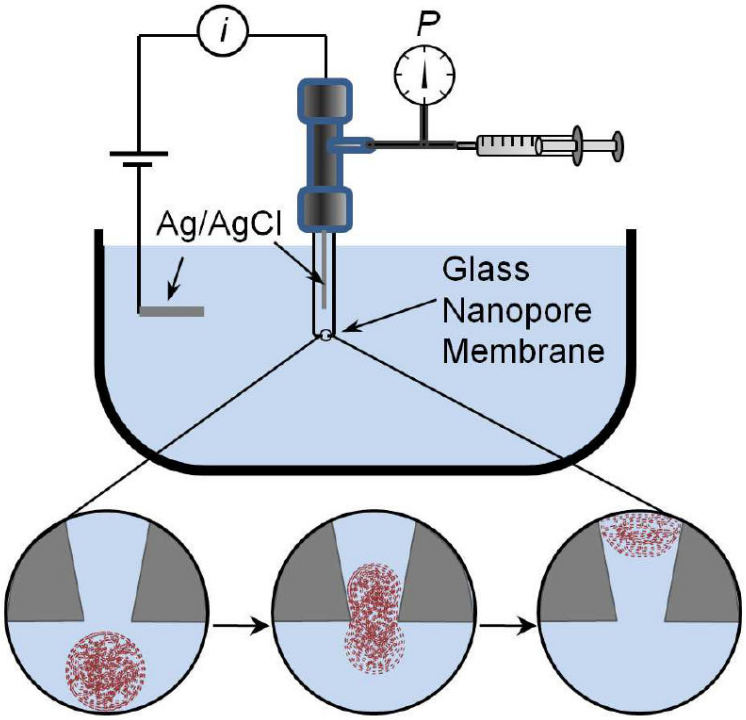

Figure 1.

Schematic drawing of the experimental setup and microgel deformation during translocation. The glass nanopore membrane (GNM) contains a single nanopore separating two electrolyte solutions. A pressure applied across the GNM drives the external electrolyte solution containing the microgels through the nanopore. A constant voltage is applied between the Ag/AgCl electrodes to record the *i-t* trace.

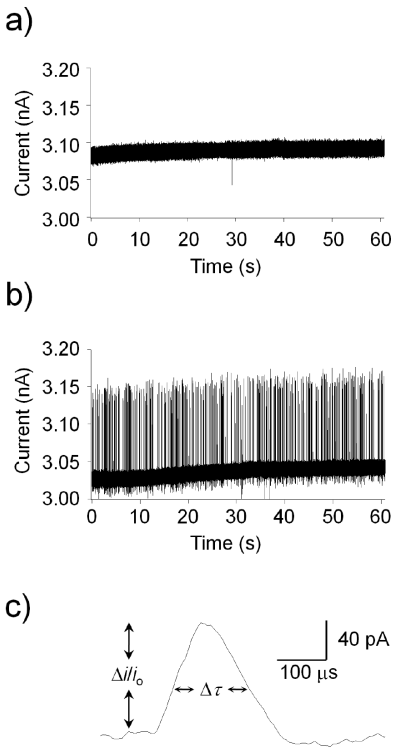

Figure 2.

Example *i-t* traces of 570-nm radius particle translocation events. Traces correspond to data obtained with a 433-nm radius pore. A background trace, in the absence of particles, is shown in (a). Particles (0.001 wt%) are driven into the pore using a pressure of −50 mmHg applied across the glass nanopore membrane (internal vs. external). Translocation events over a 60-s period are presented in (b). Expanded image of a single event is shown in (c). The open-pore current (i_o), resistive pulse peak height (μi), and width at half-peak height ($\Delta \tau$) are indicated on the figure.

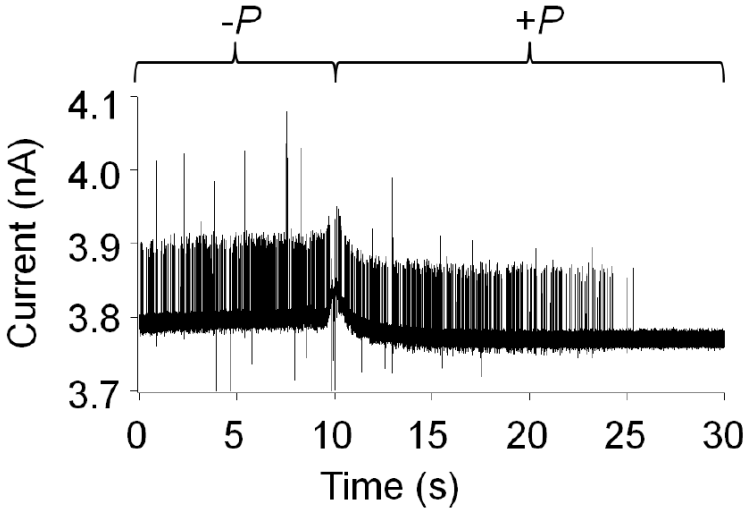

Figure 3.

Example *i-t* trace of particle translocation at *–P* and reverse translocation at *+P*. Particle translocation through a 466-nm radius pore, with an applied voltage of +0.1 V. Applied pressure was changed from −50 mmHg to +50 mmHg at time t ≈ 9 s.

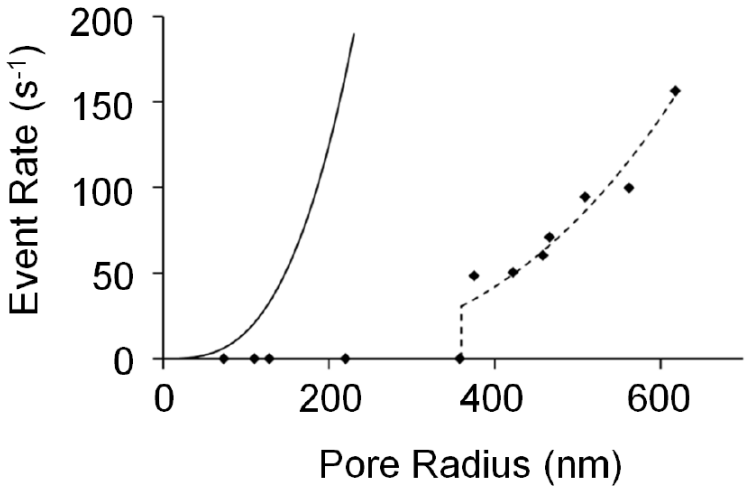

Figure 4.

Plot of the translocation event rate (events/s) as a function of the nanopore radius. All measurements were made in 0.01 M KCl solutions in a 0.001 wt% particle solution, with an applied voltage and pressure of +0.1 V and −50 mmHg, respectively (internal vs. external). Solid line (—) is analytical theory based on pressure driven translocation. Dashed line (- - -) is analytical theory multiplied by best-fitted constant (0.0418).

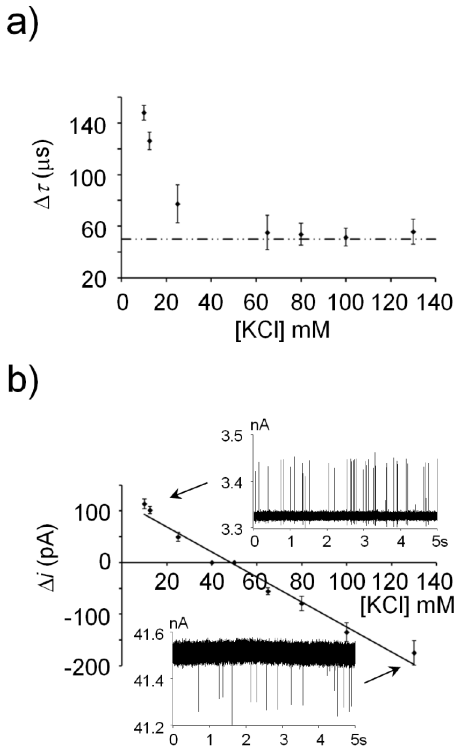

Figure 5.

Plot of (a) duration time, and (b) resistive-pulse height as a function of electrolyte concentration. All measurements were made with 0.001 wt % particles, and applied voltage and pressure of +0.1 V and −50 mmHg (internal vs. external). Dashed line in (a) represents electronic limitations due to low-pass filter. Insets in (b) show *i-t* traces of particle translocation events.

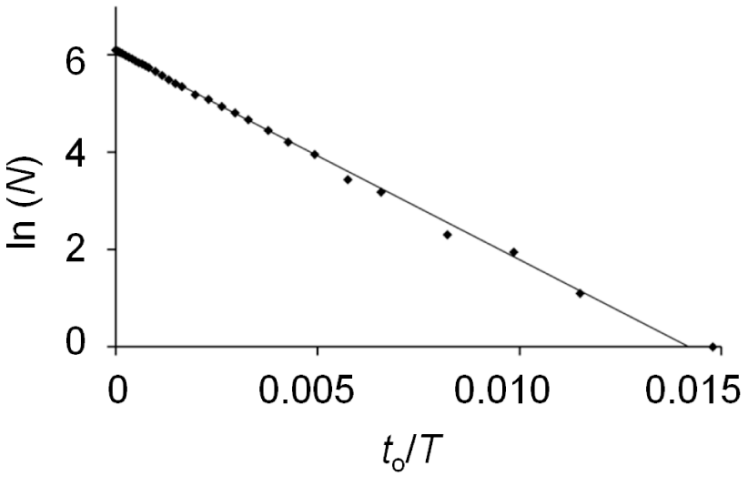

Figure 6.

Plot of ln(*N*) vs. t_0/T from data described in Figure 2(b). Total observation time, *T*, was 60.85 s yielding 443 particle translocation events. The line is a linear regression fit to the data.

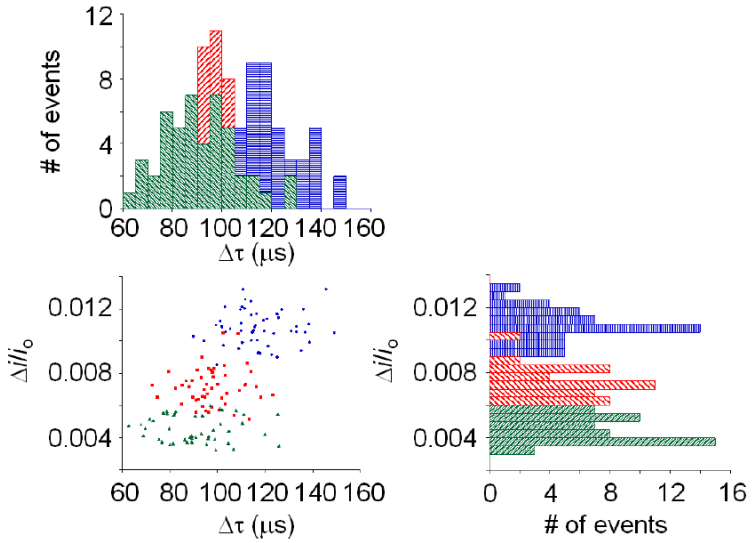

Figure 7.

Distribution of relative pulse heights ($\mu i/i_o$) vs. duration times ($\Delta\tau$) of individual translocation events through 375- (○), 509- (□), and 618- (Δ) nm radius pores (N = 50 events for each measurement). A cluster plot of $\mu i/i_o$ vs. $\Delta\tau$ for individual events is shown in lower left. Histograms of $\Delta\tau$ and $\mu i/i_o$ for the same data set are shown at the top and to the right side, respectively.